Desalination and Water Treatment
www.deswater.com
doi: 10.5004/dwt.2020.26150

202 (2020) 61–70
October

Effect of iron salt modification on the adsorption of hydrogen sulfide by sludge-based activated carbon

Fan Zeng[a], Xiaofeng Liao[b], Jiawei Lu[c], Danping Pan[d], Qili Qiu[d], Keqiang Ding[a], Wendi Zhang[d,*]

[a]*Institute of Soil and Solid Waste Pollution Control, School of Environmental Engineering, Nanjing Institute of Technology, No. 1 Hongjing Avenue Jiangning Science Park, Nanjing, Jiangsu 211167, China, emails: zf85@njit.edu.cn (F. Zeng), 2838161224@qq.com (K. Ding)*
[b]*School of Environment, China University of Geosciences, No. 388 Lumo Road, Wuhan, Hubei 430074, China, email: 575784633@qq.com (X. Liao)*
[c]*South China Institute of Environmental Sciences, MEE, No. 7 Yuancun West Street, Tianhe District, Guangzhou 410665, China, email: jiaweilu@hust.edu.cn (J. Lu)*
[d]*School of Environmental Engineering, Nanjing Institute of Technology, No. 1 Hongjing Avenue Jiangning Science Park, Nanjing, Jiangsu 211167, China, Tel. +86-25-86118973; emails: fanfuzi3@sina.com (W. Zhang), pandp@njit.edu.cn (D. Pan), qql@njit.edu.cn (L. Qiu)*

Received 25 December 2019; Accepted 23 May 2020

ABSTRACT

Sludge-based activated carbons (SACs) prepared from sewage sludge and corn straw with potassium hydroxide activation were modified with six different metal salts, and the H_2S removal performance of the modified SACs was studied. The results showed that iron salt modification shows the good effect and can improve the H_2S removal performance of the modified SAC, and that the optimum modifier is ferric nitrate. Through an orthogonal experiment, the optimum modification conditions were determined: the ferric nitrate concentration was 1.0 mol/L, the impregnation ratio was 1:4, the carbonization time was 90 min, and the carbonization temperature was 200°C. The modified SAC yielded a breakthrough sulfur capacity and saturation sulfur capacity of 27.21 and 49.17 mg/g, which were as 4.68 and 7.02 times as large as those before modification, respectively. Additionally, the results show that the carbonization temperature was the most important factor affecting the H_2S adsorption capacity of the modified SACs. The modification process increased aromatic ring structures and iron oxides (such as Fe_2O_3); those changes were all conducive to improving the chemical adsorption capacity of the modified SACs.

Keywords: Sewage sludge; Sludge based activated carbons; Metal salt modification; H_2S removal performance; Chemical adsorption capacity

1. Introduction

Sewage sludge (SS) is the main by-product of urban domestic sewage treatment plants, has an abundant reserve, and is regarded as solid waste, and the quantity of SS produced tends to increase annually with the rapid process of urbanization [1]. According to Chinese statistics, the total annual production of SS (80% moisture content) in China exceeded 40 million tons in 2017, and it is expected to reach 60 million tons in 2020 [2]. However, during the early stage of environmental protection work in China,

* Corresponding author.

research focused more on sewage treatment than sludge treatment, as a result of which more than 80% of SS is not properly disposed of, producing a large amount of secondary pollution. For example, because improper treatment has caused increasing environmental pollution, such as heavy metal pollution [3,4], odor [5], dioxin pollution [6], and pollution migration [7,8], and even hold up the sustainable development of the economy. At present, the remediation methods for SS in China mainly include sanitary landfills (approximately 65%), composting for agricultural use (approximately 15%), natural drying (approximately 6%), sludge incineration (approximately 3%), and other methods (approximately 11%) [9]. The treatment and disposal of SS normally account for approximately 25%–65% of the total operational costs of urban domestic sewage treatment plants [10]. Therefore, finding an economically viable and environmentally beneficial technological solution for the treatment of SS is one of the most pressing environmental problems that needed to be resolved in the development of modern cities.

During the wastewater treatment process, 30%–50% of the COD and 40%–70% of the organic matter in sewage are converted into SS, which makes SS appear "unstable" and act as a concentrated source of "biomass resources" and "nutrient elements." Thus, SS is a "carbon resource" with high carbon content and is a relatively suitable source of carbon. In recent research literature, some researchers aimed to produce sludge-based activated carbon (SAC) from SS [11,12].

The preparation of SAC from SS has been proven by many scholars, which has further expanded the methods of SS resource utilization. The use of SAC as an adsorption material is mainly based on two points: first, SAC has a huge specific surface area and rich pore structure, which is conducive to the physical adsorption of adsorbates by the SAC; and second, the rich surface functional groups are beneficial to the chemical adsorption of adsorbates [13]. However, some researchers have suggested that the high sand content in SS has a serious negative impact on the specific surface area and pore structure of SAC, leading to a low yield, and the corresponding adsorption performance is much lower than that of other activated carbons (ACs) prepared from biomass materials [14]. Therefore, to obtain SAC with abundant pore structures and high surface area, several auxiliary biomass materials with high carbon content have been used as carbonizers, such as agricultural waste [15–17], bagasse wastes [18], peanut hulls [19,20], and sawdust [21]. Several other researchers have used corn stalk as raw material to prepare AC [22,23]. However, studies that report the use of corn straw as a carbonizer to prepare SAC are scarce.

These high-quality SACs can be used as desulfurizers to remove H_2S. At present, the main methods of H_2S removal are dry desulfurization and low-temperature wet washing desulfurization [24], while dry desulfurization has the substantial advantage of saving energy and water resources, and has attracted more attention for H_2S removal [25,26]. In general, metal oxides (mainly iron oxide and zinc oxide) and AC are used as dry desulfurizers. However, to reduce the cost of desulfurization and realize waste recycling, SACs with abundant pore structures and high surface area are considered to be a suitable substitute.

Preliminary studies have reported that the pore structure and physicochemical properties of SAC are the key factors affecting its desulfurization performance, while the preparation process has a direct impact on the physicochemical properties of SAC [27–29]. However, some other studies have reported that a higher carbonization temperature during the preparation process would yield an SAC with high desulfurization performance; generally, such carbonization temperatures are over 950°C [30]. Considering energy consumption, reducing the carbonization temperature without affecting the desulfurization performance will be more conducive to the industrial application of SAC.

Ansari et al. [31] prepared SAC from SS and high polymer to remove H_2S and found that high polymer was a better carbonizer when the mass ratio of SS to carbonizer was 1:1, yielding a SAC obtained with the best desulfurization performance among those of the studied samples. However, excessive content of carbonizer would weaken the buffering capacity for surface acid functional groups, which have an obvious inhibitory effect on the adsorption of H_2S. Wallace et al. [32] used fish waste as a carbonizer to prepare SAC and found that an excessive content of carbonizer was not conducive to the adsorption ability of H_2S. Additionally, the above article reported that the active component Fe in SS has a positive effect on the H_2S adsorption ability of SAC. Wang et al. [33] also reported that metal doping would increase the desulfurization ability of SAC. Others articles have reported that metal oxides on the surface of SAC are conducive to its adsorption capacity. Bagreev et al. [30] and Bagreev and Bandosz [34] suggested that metal oxides, such as ZnO, CaO, CuO, and Fe_2O_3, on the surface of SAC are conducive to the adsorption of H_2S.

Thus, some researchers have carried out metal loading modification studies on SAC for the purpose of improving the adsorption performance of SAC, especially the selective adsorption ability [35]. After modification with iron salt, the modified SACs presented a more developed pore structure, as well as increased the specific surface area and pore volume. Zhai [36] modified SAC with several metal materials, and the results showed that the optimal supporting metal materials were vanadium and iron, which increased the adsorption capacity of the SAC by 106% and 75%, respectively. Ge [37] compared the effect of different metal salt modifiers, such as $Fe(NO_3)_3$, $FeCl_3$, $Cu(NO_3)_2$, and $CuCl_2$, on the adsorption performance of SAC and found that the adsorption performance of iron-modified SAC was more stable than that of other SAC samples. Generally, transition metals or transition metal compounds are chosen as metal modifiers.

In the preliminary studies, a series of SACs were prepared and the H_2S adsorption properties were discussed. In this work, pre-prepared SACs were modified with six different metal salts, and the desulfurization performances of the modified SACs were studied. Thus, the main objective of this work was to (1) investigate the possibility of increasing the desulfurization capacity of SAC by metal salt modification and find the best modifier and (2) analyze the influence of metal salt modification on the adsorption properties of SAC and find the optimal modification conditions. This study proposes a novel desulfurizer prepared from

the low-cost and widespread source of raw materials and explores the potential of SAC as an adsorbent.

2. Materials and methods

2.1. Feedstock materials

In the preliminary experimental study, a series of SACs were prepared from SS and corn straw by potassium hydroxide activation, and the desulfurization performance of the SACs were studied [27–29]. The results showed that a mass ratio of SS, corn straw, and potassium hydroxide of 3:7:2, referred to as SAC372, yielded the best breakthrough and saturation sulfur sorption capacities of 5.82 and 7.00 mg H_2S/g SAC, respectively [27]. Therefore, SAC372 was selected as the target for modification in this study. H_2S standard gas was purchased from Wuhan Nuerui De Trade Co., Ltd. (Wuhan, China), the H_2S gas concentration was 2,000 ppm, and the equilibrium gas was N_2. All chemicals used in this study were of analytical grade.

2.2. Modified preparation of SAC

Metal salts including $Cu(NO_3)_2$, $Zn(NO_3)_2$, $Mn(NO_3)_2$, $Fe(NO_3)_3$, $Fe_2(SO_4)_3$, and $FeCl_3$, were selected as modifiers to modify SAC372. The modification experiment steps were as follows.

Step 1: A 10.000 g quantity of SAC372 was accurately weighed into iodine flask (with stopper), the above-mentioned modifiers were added at a concentration of 1 mol/L according to an impregnation ratio of 1:4 (g/mL), and the flask was well mixed. However, to maintain the same Fe^{3+} concentration in the iron salt modifiers, the concentration of $Fe_2(SO_4)_3$ was 0.5 mol/L. *Step 2*: The stoppered iodine flask was placed on a shaker at a rate of 120 r/min for 6 h, and then the impregnated samples were transferred into ceramic crucibles and dried at 80°C in an electro-thermostatic blast oven for 24 h. *Step 3*: The dried impregnated samples were then subjected to a pyrolysis process in a controlled atmosphere box furnace (QXR1200-30, manufactured by Shanghai Qian Tong Technology Co., Ltd. (Shanghai, China). Under an atmosphere of nitrogen, the internal temperature of the furnace was heated to 400°C at a speed of 5°C/min, and the temperature was kept constant for 60 min. After pyrolysis, the furnace was cooled to room temperature under the same nitrogen atmosphere. *Step 4*: The carbonized samples were continuously washed with hot distilled water (80°C) until the pH of the filtrate reached approximately 7 and then dried at 80°C to a constant weight to obtain the modified SAC. Each experiment was carried out in triplicate. The SACs modified with $Cu(NO_3)_2$, $Zn(NO_3)_2$, $Mn(NO_3)_2$, $Fe(NO_3)_3$, $Fe_2(SO_4)_3$, and $FeCl_3$ were denoted as SAC372-CuN, SAC372-ZnN, SAC372-MnN, SAC372-FeN, SAC372-FeS, and SAC372-FeCl, respectively.

2.3. Desulfurization experiment

The desulfurization experiments were carried out with the above-mentioned modified SAC372 samples and SAC372 as the desulfurization agents. The desulphurization experiments were performed as described in previous articles published by our group, and the experimental apparatus flow chart of H_2S adsorption is shown in Fig. 1.

The above SACs were further ground to a particle size of less than 0.3 mm for use as desulfurization agents. The experimental adsorption device was a homemade muffle furnace that consisted of a temperature control device, an adsorption chamber, a pressure stabilizing device, a tail gas treatment device, and a tail gas detection device. The adsorbent chamber was a quartz tube with a diameter of 11 mm, and both ends of the quartz tube were blocked with absorbent cotton. The pressure stabilizing device comprised two parts: a flow meter (FL-3013SA, Omega, Norwalk, State of California, USA) and a surge chamber were used in series to ensure a stable air pressure before entering the gas conduit, and a micro-adjusting needle valve (WL31H-320P-DW8) and another flow meter were used in series after the surge chamber to control the flow rate and the pressure of the gas before entering the adsorbent chamber.

SAC (2.000 g) was accurately weighed into the quartz tube, the H_2S flow rate was 100 mL/min, and the adsorption temperature was constant at 50°C. The H_2S removal efficiency of the SAC samples was evaluated by the breakthrough sulfur capacity (Q_B) and saturation sulfur capacity (Q_S), which were calculated by measuring the spectrophotometric value of S^{2-} in the absorption liquid at different times with p-amino dimethyl aniline method. Generally, the breakthrough time (T_B) is defined as the time at which the ratio of the outlet concentration to the inlet concentration (C_t/C_0) is 5%, and the corresponding sulfur capacity is the breakthrough sulfur capacity; the saturation time is defined as the time at which C_t/C_0 is 95%, and the corresponding sulfur capacity is the saturated sulfur capacity. The formula used to calculate Q_B and Q_S is as follows:

$$Q = \frac{qM}{wV_m}\left(C_0 t - \int_0^t C_t dt\right) \times 10^{-6} \quad (1)$$

where Q is the sulfur capacity of the desulfurizer (mg H_2S/g desulfurizer); M is the molar mass of H_2S (34 g/mol); V_m is the gas molar volume constant (22.4 L/mol); q is the flow of inlet gas (L/min); t is the breakthrough time/saturation time (min); w is the mass of the desulfurizer (g); C_0 is the inlet concentration of H_2S (ppm); C_t is the outlet concentration of H_2S (ppm).

2.4. Characterization

The physical parameters of SACs were analyzed by using an automatic specific surface area and porosity analyzer (JW-BK122W, JWGB Ltd., China). The weight loss behavior of samples was carried out with a diamond TG/DTA instrument (PerkinElmer Instruments, USA). The temperature was heated up to 1,000°C in the N_2 atmosphere with a 100 mL/min flow rate, while the heating rate was 10°C/min. The structures and functional groups of the samples were analyzed by Fourier transform infrared spectroscopy (FT-IR) (Bruker VERTEX 70, German). The crystallographic microstructure of SAC samples was analyzed by using X-ray diffractometer (XRD) (X'Pert PRO, PANalytical B.V., Holland), which was carried out at a scanning diffraction angle of 10°–80°.

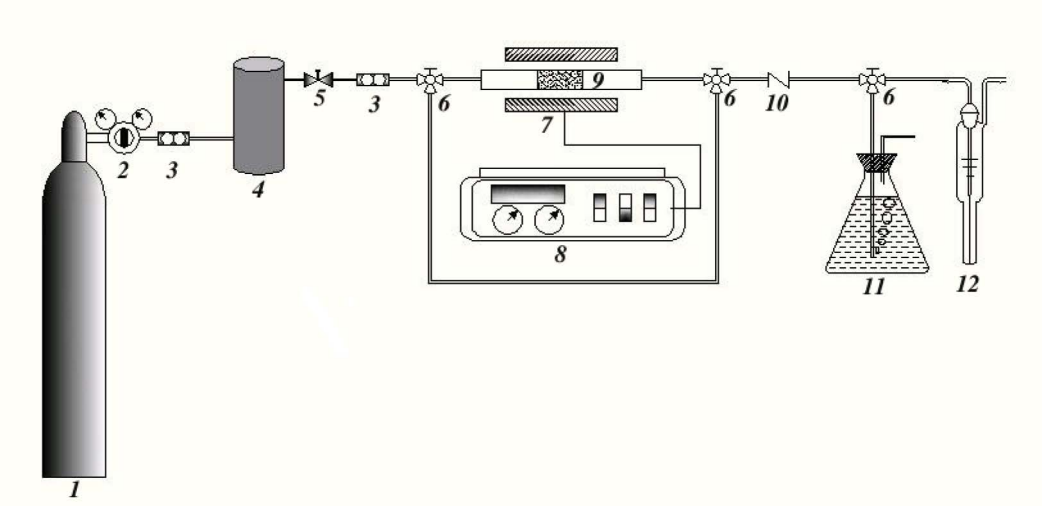

Fig. 1. Experimental apparatus flow chart of H_2S adsorption. (1) Hydrogen sulfide cylinder, (2) pressure reducer, (3) flow meter, (4) surge chamber, (5) needle valve, (6) triple valve, (7) temperature controller, (8) tube furnace, (9) samples of adsorption chamber, (10) single-directioned valve, (11) tail gas absorber, and (12) bubble absorption tube.

3. Results and discussion

3.1. Effect of different modifiers on desulfurization performance

The effect of different modifiers on the desulfurization performance of the SACs was investigated. The results for T_B and the corresponding Q_B and Q_S values of H_2S for different SACs are shown in Table 1.

As shown in Table 1, among the six modifiers, only $Fe(NO_3)_3$ and $FeCl_3$ increased the desulfurization performance of the SACs, other modifiers decreased the desulfurization performance. The T_B, Q_B, and Q_S of SAC372 were 100 min, 5.82, and 7.00 mg H_2S/g SAC, respectively. The T_B of SAC372-FeN increased to 170 min, 1.7 times longer than that of SAC372. Correspondingly, the Q_B and Q_S of SAC372-FeN were 12.89 and 15.69 mg H_2S/g SAC, representing increases of 121.48% and 124.14%, respectively. The T_B, Q_B, and Q_S of SAC372-FeCl were 130 min, 7.59 and 11.64 mg H_2S/g SAC, representing increases of 30%, 30.41%, and 66.29%, respectively. The results showed that the desulfurization performance of SAC samples prepared from SS in this experiment is close to that of commercial wood-based activated carbon (CAC). Chen and Lai [38] modified CAC with ferric nitrate, and obtained a H_2S removal performance of 19.60 mg H_2S/g CAC. Zhang et al. [39] modified CAC with ferric chloride, and the optimal adsorption capacity for H_2S was 14.20 mg H_2S/g CAC. However, given the adsorption performance of other materials, this capacity can still be substantially improved. For instance, Pipatmanomai et al. [40] impregnated CAC with 2% potassium iodide, and the modified CAC yielded an adsorption capacity of 62 mg H_2S/g CAC.

Wallace et al. [32] believed that increasing the iron content in SACs could help increase their desulfurization performance. From this point of view, the desulfurization performance of all three SACs modified with ferric salts should be higher than that of SAC372. However, the desulfurization performance of SAC372-FeS which was modified with $Fe_2(SO_4)_3$, declined, with T_B declining by 50% and Q_B and Q_S declining by 47.77% and 28.57%, respectively.

To better understand the effect of iron salt modification on the desulfurization performance, SAC372-FeN, SAC372-FeS, and SAC372-FeCl were selected as the study subjects. The adsorption performance of AC is related to the surface area and pore structure, which can be reflected by the N_2 adsorption/desorption isotherm and pore size distribution.

Fig. 2 shows the pore size distribution of the three modified SACs and SAC372. The evident type-IV isotherms and the hysteresis loop in the adsorption/desorption isotherms indicate the existence of mesoporous structures in the samples [41]. As shown in Fig. 2, after modification with different iron salts, the pore structure of the three modified SACs was reduced, and the reduction trend of SAC372-FeS was the most obvious. To make a clear comparative analysis, the pore diameter distribution data for the above four kinds of SACs are listed in Table 2.

Table 2 shows the pore structure parameters of the four SACs. It can be seen from the results that the specific surface area (S_{BET}) of SAC372-FeS decreased sharply by 97.11% and the blocked or destroyed pore structure of SAC372-FeS mainly comprised micropores, whose specific surface area decreased by 97.07%, leaving only a small amount of macroporous structure. Generally known that $Fe_2(SO_4)_3$ is practically sparingly soluble in water, and the decomposition temperature is 480°C. Thus, in the process of modifying SAC372, $Fe_2(SO_4)_3$ is not evenly dispersed to the surface of SAC372, and $Fe_2(SO_4)_3$ is not completely melted and decomposed at the carbonization temperature of 400°C, which both blocked the original pore structure. Thus, the above phenomenon greatly reduced the physical adsorption capacity, which led to a decrease in the desulfurization performance of SAC372-FeS.

It is known that a reduction in pore structure leads to a decrease in adsorption capacity [42,43]. However, as shown in Table 1, there were abnormal growth trends in desulfurization performance for both SAC372-FeCl and SAC372-FeN.

Table 1
Desulfurization performance of different SACs

Desulfurizer* and desulfurization performance	SAC372	SAC372-CuN	SAC372-ZnN	SAC372-MnN	SAC372-FeN	SAC372-FeS	SAC372-FeCl
T_B (min)	100 ± 3**	70 ± 1	60 ± 1	90 ± 3	170 ± 3	50 ± 1	130 ± 3
Q_B (mg/g)	5.82 ± 0.029	4.73 ± 0.024	3.71 ± 0.019	5.13 ± 0.025	12.89 ± 0.059	3.04 ± 0.014	7.59 ± 0.028
Q_S (mg/g)	7.00 ± 0.035	6.59 ± 0.031	5.94 ± 0.027	6.84 ± 0.029	15.69 ± 0.071	5.00 ± 0.023	11.64 ± 0.054

*SAC372-CuN, SAC372-ZnN, SAC372-MnN, SAC372-FeN, SAC372-FeS, and SAC372-FeCl were the SAC372 modified by $Cu(NO_3)_2{\cdot}3H_2O$, $Zn(NO_3)_2{\cdot}6H_2O$, $Mn(NO_3)_2{\cdot}6H_2O$, $Fe(NO_3)_3{\cdot}9H_2O$, $Fe_2(SO_4)_3{\cdot}9H_2O$, and $FeCl_3{\cdot}6H_2O$, respectively. T_B: breakthrough time; Q_B: breakthrough sulfur capacity; Q_S: saturation sulfur capacity; **Error ranges is the standard deviation.

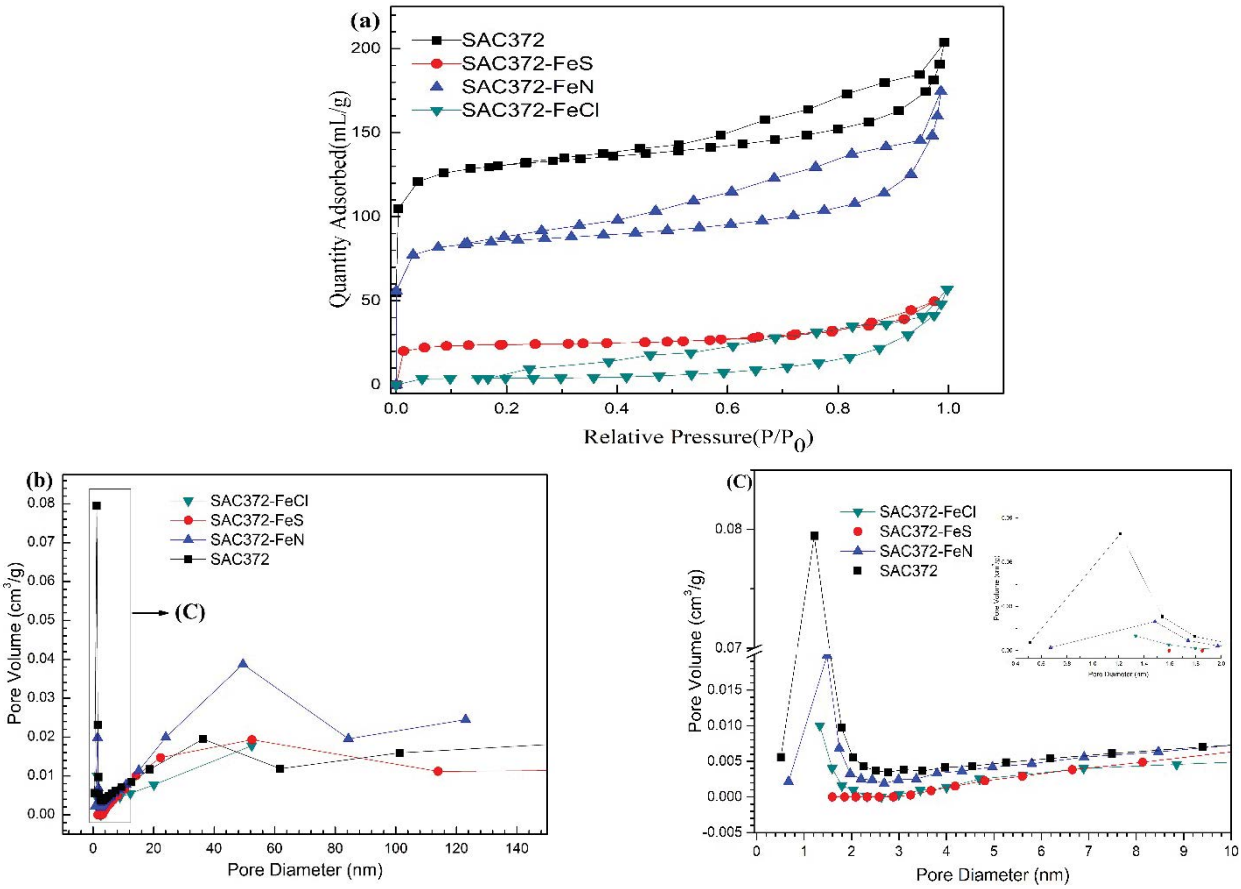

Fig. 2. (a) N_2 adsorption/desorption isotherms of different SACs, (b) pore size distributions of different SACs (0–150 nm), and (c) pore size distributions of different SACs (0–10/0–2 nm).

The pore structure of SAC372-FeCl was also obviously reduced, losing 77.38% of its total pore volume (V_{total}), and the blocked or destroyed pore structure of SAC372-FeCl mainly comprised micropores, whose pore volume decreased by 83.09%. This dramatic loss phenomenon may be due to the thermal decomposition of $FeCl_3$ at the carbonization temperature of 400°C. Decomposition products such as Fe_2O_3 and Fe_3O_4 could block the original pore structure [44,45]. Thus, during the modification process, the physical adsorption capacity of SAC372-FeCl was greatly reduced; however, the pyrolysis products and undecomposed modifiers could adsorb H_2S, which enhanced the chemical adsorption ability and led to an increase in the desulfurization performance of SAC372-FeCl.

During the modification process, $Fe(NO_3)_3$ decomposed into Fe_2O_3, NO_2, O_2, and other substances after being heated. Fe_2O_3 would block part of the original pore structure, while NO_2 and O_2 would expand the pore structure in SAC372-FeN. However, it can be seen from Fig. 2 and Table 2 that the pore expansion effect could not offset the blocking of

Table 2
Pore structure parameters of different SACs

Adsorbent	S_{BET} (m^2/g)	V_{total} (cm^3/g)	D_{ave} (nm)	V_{micro} (cm^3/g)	I
SAC372	462.931	0.367	3.172	0.2318	0.6316
SAC372-FeS	13.383	0.100	29.875	0.0068	0.068
SAC372-FeCl	83.326	0.083	3.968	0.0392	0.4723
SAC372-FeN	382.345	0.286	4.047	0.1369	0.4787

S_{BET}, BET surface area; V_{total}, total pore volume; D_{ave}, average pore diameter; V_{micro}, micropores volume; I, microporosity, defined as V_{micro}/V_{total}.

the pore structure, so the S_{BET} and V_{total} of SAC372-FeN were reduced. On the other hand, the added substance Fe_2O_3 also has desulfurization ability and thus increased the chemical adsorption capacity of SAC372-FeN.

The above results showed that after the modification process, the pore structure of the modified SACs decreased, which was not conducive to the physical adsorption of H_2S. However, the desulfurization performance of SAC372-FeCl and SAC372-FeN were increased, indicating that the desulfurization of modified SAC was dominated by chemical adsorption. To further explore the reasons for the increase in desulfurization performance of the modified SACs, FT-IR analysis was carried out on the above four SACs, and the results are shown in Fig. 3.

Fig. 3a shows that all four SACs have similar stretching vibration peaks at wavenumbers of 3,400; 2,900; 1,600; and 1,100–1,000 cm^{-1}. As reported, the strong absorption band at approximately 3,400 cm^{-1} can be assigned to hydroxyl group (O–H) and/or nitrogen-containing surface group (N–H) stretching, the inconspicuous absorption band at approximately 2,900 cm^{-1} can be assigned to C–H, the absorption band at approximately 1,600 cm^{-1} can be assigned to $–COO^-$, and the absorption band observed at 1,100–1,000 cm^{-1} can be assigned to stretching vibrations of –O– [46,47]. As shown in Fig. 3b, after the modification process, the stretching vibration peaks exhibit evident differences in detail from 1,100 to 1,000 cm^{-1}. The intensities of the absorption bands at 1,100–1,000 cm^{-1} in SAC372-FeS and SAC372-FeN were higher than those of the characteristic diffraction bands of SAC372, and the intensity of the absorption bands in SAC372-FeS was the highest. The above –O– groups correspond to the oxygen-containing bonds in lactone groups, which are not conducive to the desulfurization performance of SAC [43]. Therefore, the desulfurization performance of SAC372-FeS was significantly inhibited.

Moreover, there were stretching vibration peaks for C=C (1,400 cm^{-1}) and associated C–H (700 cm^{-1}) in the SAC372-FeN, which were not observed in the other three SAC samples. Khoshbouy et al. [48] suggested that C=C at around 1,400 cm^{-1} was derived from aromatic ring structure. The results indicate that after modification with $Fe(NO_3)_3$, the aromatic ring structures in SAC372-FeN increased, or maybe formed new microcrystalline structures, which improved desulfurization performance. In addition, comparing the absorption peaks of the four samples showed that new asymmetric stretching vibrations of Fe–O appeared in SAC372-FeS (590 cm^{-1}) and SAC372-FeN (560 cm^{-1}). However, as the residual modifier SO_4^{2-} in SAC372-FeS has a high contribution rate to the absorption peak of Fe–O, the

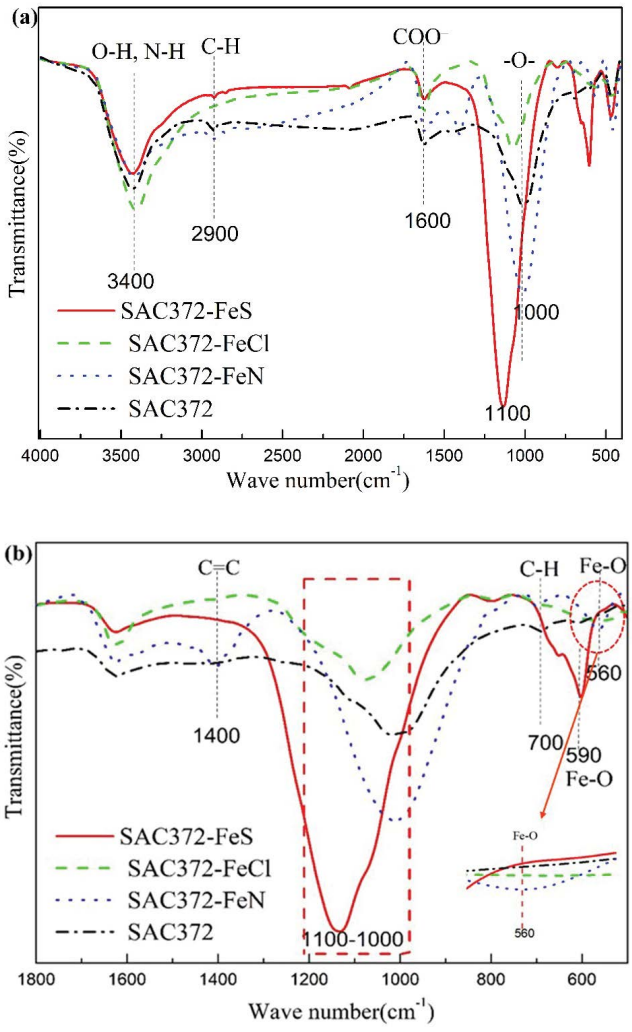

Fig. 3. FT-IR spectrograms of different ACs (a) 4,000–400 cm^{-1} and (b) 1,800–500 cm^{-1}.

absorption peak of SAC372-FeS at 590 cm^{-1} was relatively obvious [49,50]. This result indicated that the new product iron oxide was formed in SAC372-FeN.

The above results showed that the modifier had a significant improvement effect on the surface functional groups of SACs, to a certain extent, this effect could compensate for the negative effect on the pore structure destruction of SACs and even improve the desulfurization

performance of the SACs. Among the three modification agents, $Fe(NO_3)_3$ has the best ability to improve the desulfurization performance of SAC. The $Fe(NO_3)_3$ modification process had a less negative effect on the SAC pore structure, and the by-products of thermal decomposition could promote the chemical desulfurization performance of SAC372-FeN; thus, the desulfurization performance of SAC372-FeN was significantly improved.

The desulfurization performance of SACs is also affected by the crystal structure. To further verify the conclusions obtained above, the four SACs were selected for XRD analysis, and the results are shown in Fig. 4.

As shown in Fig. 4, the XRD spectra of the SACs prepared in this experiment do not show any obvious X-ray diffraction peaks, and only several weak peaks can be observed. The results showed that the crystallization degree on the surface of the above SACs was not high, and the content was also low. Dehydrated sludge, one of the raw materials used, has complex components, including various metals, resulting in the poor crystal structure of SACs prepared by the mixed pyrolysis of sludge and corn straw.

Additionally, as shown in Fig. 4, in the XRD spectra of the above four SACs, there were diffraction peaks of Si at 2θ of approximately 29°. Except for SAC372-FeS, all of the SACs showed the presence of $CaCO_3$ at 2θ of approximately 40° [51]. The spectra of SAC372 showed several diffraction peaks, which can be assigned to SiO_2 (at 2θ of approximately 20°), Si, and Fe_2O_3 (at 2θ of approximately 33°).

However, the XRD patterns of SACs modified with different iron salts were different. In the XRD spectrum of SAC372-FeS, peaks of Fe_2O_3 can be observed at 2θ of both 24° and 33°, while in the XRD spectrum of SAC372-FeN, peaks of Fe_2O_3 can be observed at 2θ of 35°, 57°, and 63°. Moreover, after modification with iron salt, the diffraction intensity of Si weakened, and the spectrum of SAC372-FeN did not show an obvious Si diffraction peak. The above-mentioned phenomenon suggested that modification with iron salt could destroy some of the Si crystal structure while introducing another new Fe_2O_3 crystal structure on the surface of SAC. The modification process of ferric nitrate was more obvious. In general, the Si crystal structure in SAC formed part of its internal pore structure. The above conclusion further verified that the modification of iron salt destroyed the original pore structure of SAC372 while generated some new pore structure, and new Fe_2O_3 crystal structure in SAC372-FeN. However, the contribution of new pores to hydrogen sulfide adsorption capacity of SAC372-FeN is lower than that of Fe_2O_3.

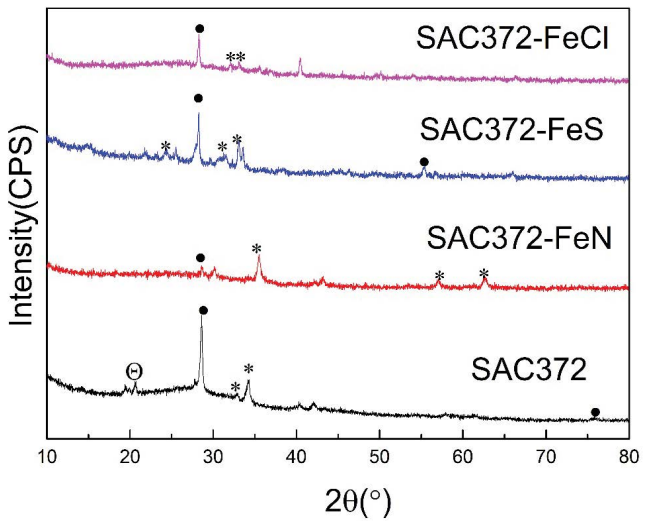

Fig. 4. XRD spectra of different SACs (ΘSiO_2, *Fe_2O_3, and •Si).

3.2. Effect of ferric nitrate modification on desulfurization performance

The above conclusion indicates that modification with ferric nitrate has the best effect on improving the desulfurization performance of SACs. To verify this conclusion, ferric nitrate was used as the target modifier for further study. In this experiment, orthogonal design was introduced into the modification process, and an orthogonal experiment with four factors and four levels was designed to sift out the optimized conditions. Thus, 16 kinds of SAC were prepared for the above orthogonal experiment, the parameters included the concentration of ferric nitrate (denoted as *A*; the values were 0.5, 1.0, 1.5, and 2.0 mol/L), impregnation ratio (denoted as *B*; the value were 1:1, 1:2, 1:3, and 1:4 g/mL), carbonization time (denoted as *C*; the value were 30, 60, 90, and 120 min), and carbonization temperature (denoted as *D*; the value were 100°C, 200°C, 300°C, and 400°C). The pore structure parameters and the corresponding Q_B and Q_S of H_2S for different SAC372-FeN samples were investigated, and the results are shown in Table 3.

As shown in Table 3, SAC372-FeN-8 yielded the best desulfurization performance, and its Q_B and Q_S were 27.21 and 48.10 mg/g, 4.68 and 7.02 times those before modification, respectively. After modification with ferric nitrate, the desulfurization performance of SAC372-FeN-8 was significantly improved.

Additionally, taking Q_S as index, the experimental data were analyzed by range analysis (represented the measures of variation in statistical data) and variance analysis (ANOVA, analysis of variance, determined the significance of each influencing factor), and the results showed that the above four factors affecting the saturated sulfur capacity of SAC, from strong to weak, were in the order of carbonization temperature, carbonization time, impregnation ratio, and concentration of ferric nitrate. The results indicated that the chief factor influencing the desulfurization performance of SAC372-FeN was the carbonization temperature. Therefore, taking into account the carbonization temperature, SAC372-FeN5, SAC372-FeN6, SAC372-FeN7, and SAC372-FeN8, which were prepared at 100°C, 200°C, 300°C, and 400°C, respectively, were selected for FT-IR analysis, and the results are shown in Fig. 5.

From Table 3, the saturated sulfur capacity of SAC, from low to high, was in the order of SAC372-FeN6 (400°C), SAC372-FeN5 (300°C), SAC372-FeN7 (100°C), and SAC372-FeN8 (200°C). As shown in Fig. 5, the above four modified SACs have similar FT-IR spectrograms; however, the FT-IR shifts and intensities of the vibrations were affected by carbonization temperature. As the carbonization temperature increases, the intensity of the main characteristic peaks of the

infrared spectra first increases and then decreases, while the saturated sulfur capacity of SAC exhibits a similar tendency. Additionally, from Fig. 5, a new wide and split peak of C=C (approximately 1,500 cm^{-1}) and associated C–H (700 cm^{-1}) can be observed in SAC372-FeN8. As SAC372-FeN8 had the best desulfurization performance, it further verified the above conclusion that C=C and associated C–H were conducive to the improvement of desulfurization performance.

Moreover, as shown in Fig. 5, the infrared spectra of all SACs modified with ferric nitrate at different temperatures showed a new absorption peak near 560 cm^{-1}, which corresponds to Fe–O bonds. This result, combined with the XRD analysis, confirmed again that Fe_2O_3 was generated in the ferric nitrate modification process, and conducive to the improvement of desulfurization performance.

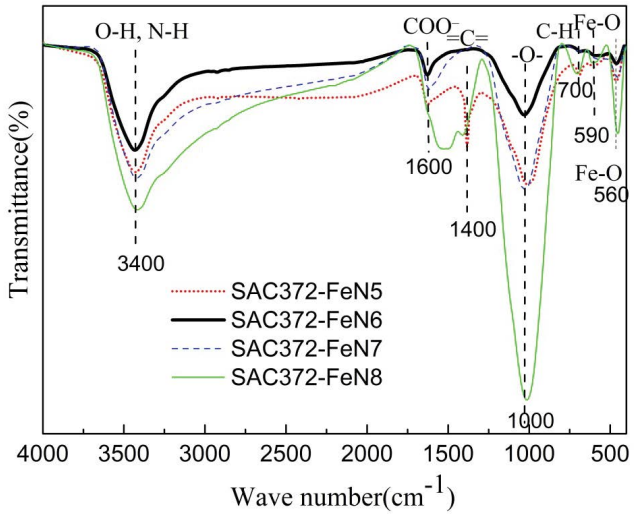

Fig. 5. FT-IR spectrograms of modified SACs prepared at different temperatures.

4. Conclusion

Sewage sludge and corn straw were successfully used to produce effective desulfurizers at a low temperature, and suitable metal salt modification further improved the desulfurization performance of the desulfurizer. The experimental research described in this work allows us to draw the following conclusions:

- After modification with $Cu(NO_3)_2$, $Zn(NO_3)_2$, $Mn(NO_3)_2$, and $Fe_2(SO_4)_3$, the desulfurization performance of the SACs decreased. However, the desulfurization performance of the SACs that modified with $Fe(NO_3)_3$ and $FeCl_3$ was improved, and $Fe(NO_3)_3$ showed the best modification effect.
- Through an orthogonal experiment, the optimum modification conditions were obtained: the $Fe(NO_3)_3$ concentration was 1.0 mol/L, the impregnation ratio was 1:4, the carbonization time was 90 min, and the carbonization temperature was 200°C. The Q_B and Q_S of the SAC prepared under the above conditions were 27.21 and 48.10 mg/g, 4.68 and 7.02 times those before modification, respectively. Additionally, the results show that the carbonization temperature was the most important factor affecting the desulfurization performance of the modified SACs.
- Modification with $Fe(NO_3)_3$ improved the chemical adsorption capacity of the SACs. After the modification

Table 3
Orthogonal design of experiment table $L_{16}(4^5)$

Samples	*A* (mol/L)	*B* (g/mL)	*C* (min)	*D* (°C)	V_{total} (cm^3/g)	D_{ave} (nm)	V_{micro} (cm^3/g)	D_{con} (nm)	S_{BET} (m^2/g)	Q_B (mg/g)	Q_S (mg/g)
SAC372-FeN1	0.5	1:1	30	100	0.301	3.055	0.1866	1.0544	393.872	6.002 ± 0.021*	11.141 ± 0.033
SAC372-FeN2	0.5	1:2	60	200	0.323	2.408	0.2490	1.0420	536.096	13.544 ± 0.061	25.836 ± 0.073
SAC372-FeN3	0.5	1:3	90	300	0.473	3.164	0.2633	1.1839	598.277	12.863 ± 0.053	24.215 ± 0.073
SAC372-FeN4	0.5	1:4	120	400	0.213	5.398	0.0759	0.5762	157.627	4.554 ± 0.016	7.160 ± 0.021
SAC372-FeN5	1.0	1:1	60	300	0.290	3.839	0.1462	1.0358	302.349	12.870 ± 0.054	14.163 ± 0.039
SAC372-FeN6	1.0	1:2	30	400	0.239	3.785	0.1207	1.0498	252.615	6.065 ± 0.024	8.533 ± 0.025
SAC372-FeN7	1.0	1:3	120	100	0.219	3.365	0.1252	1.1772	260.317	4.460 ± 0.017	16.219 ± 0.047
SAC372-FeN8	1.0	1:4	90	200	0.402	2.867	0.2673	1.4061	560.996	27.209 ± 0.101	48.098 ± 0.126
SAC372-FeN9	1.5	1:1	90	400	0.266	3.272	0.1580	1.1739	325.659	7.576 ± 0.027	13.133 ± 0.037
SAC372-FeN10	1.5	1:2	120	300	0.204	3.545	0.1080	0.7631	230.466	10.572 ± 0.039	13.861 ± 0.041
SAC372-FeN11	1.5	1:3	30	200	0.230	3.956	0.1096	0.9263	232.254	15.179 ± 0.057	20.707 ± 0.063
SAC372-FeN12	1.5	1:4	60	100	0.233	4.725	0.0853	1.0710	197.214	2.973 ± 0.009	22.174 ± 0.061
SAC372-FeN13	2.0	1:1	120	200	0.216	3.294	0.1321	0.6864	261.883	13.656 ± 0.057	17.401 ± 0.051
SAC372-FeN14	2.0	1:2	90	100	0.218	4.051	0.0941	1.0612	215.134	2.992 ± 0.007	14.866 ± 0.031
SAC372-FeN15	2.0	1:3	60	400	0.281	7.290	0.0638	1.0909	154.212	7.392 ± 0.026	19.531 ± 0.043
SAC372-FeN16	2.0	1:4	30	300	0.387	12.509	0.0464	1.2469	123.748	18.214 ± 0.049	22.845 ± 0.057

A: concentration of ferric nitrate; *B*: impregnation ratio; *C*: carbonization time; *D*: carbonization temperature; S_{BET}: BET surface area; D_{ave}: average pore diameter; V_{total}: total pore volume; V_{micro}: micropores volume; D_{con}: the most concentrative pore diameter; Q_B: breakthrough sulfur capacity; Q_S: saturation sulfur capacity; *Error ranges is the standard deviation.

process, the aromatic ring structures in SAC372-FeN increased, and iron oxides (such as Fe_2O_3) were formed; all of these effects were conducive to the improvement of desulfurization performance.

Acknowledgments

This work was supported by the Natural Science Research of Jiangsu Higher Education Institutions of China (No. 19KJB610012), the Introduction Talent Scientific Research Foundation Project of Nan Jing Institute of Technology (No. YKJ201934), and the National Key Research and Development Plan of China (No. 2017YFC0212605).

References

[1] P. Hadi, M. Xu, C. Ning, C. Sze Ki Lin, G. McKay, A critical review on preparation, characterization and utilization of sludge-derived activated carbons for wastewater treatment, Chem. Eng. J., 260 (2015) 895–906.
[2] X.H. Dai, Thoughts on the necessity and urgency of stabilizing sludge treatment in urban sewage treatment plants, Water Wastewater Eng., 53 (2017) 1–5 (in Chinese).
[3] N. Wang, Q.W. Liu, Y. Zhi, L. Cheng, B.J. Ma, Y.X. Mao, Spatial and temporal variation of mercury in municipal sewage sludge in China, Environ. Sci., 39 (2018) 2296–2305.
[4] E. Peruzzi, G. Masciandaro, C. Macci, S. Doni, S.G.M. Ravelo, P. Peruzzi, B. Ceccanti, Heavy metal fractionation and organic matter stabilization in sewage sludge treatment wetlands, Ecol. Eng., 37 (2010) 771–778.
[5] X.H. Dai, C.L. Hu, D. Zhang, Y.G. Chen, A new method for the simultaneous enhancement of methane yield and reduction of hydrogen sulfide production in the anaerobic digestion of waste activated sludge, Bioresour. Technol., 243 (2017) 914–921.
[6] S. Werle, R. Wilk, A review of methods for the thermal utilization of sewage sludge: the polish perspective, Renewable Energy, 35 (2010) 1914–1919.
[7] K. Gondek, M. Mierzwa-Hersztek, M. Kope, Mobility of heavy metals in sandy soil after application of composts produced from maize straw, sewage sludge and biochar, J. Environ. Manage., 210 (2018) 87–95.
[8] J.H. Li, M. Zhang, Z.Y. Ye, C.M. Yang, Effect of manganese oxide-modified biochar addition on methane production and heavy metal speciation during the anaerobic digestion of sewage sludge, J. Environ. Sci., 76 (2018) 267–277.
[9] H. Lian, Sludge Disposal Status and Control Countermeasures, 2016 Sludge Summit Forum, 3rd ed., Henan, Zhengzhou, 2016 (in Chinese).
[10] N. Mu'Azu, N. Jarrah, M. Zubair, O. Alagha, Removal of phenolic compounds from water using sewage sludge-based activated carbon adsorption: a review, Int. J. Environ. Res Public Health, 14 (2017) 1–34.
[11] M.A. Franciski, E.C. Peres, M. Godinho, D. Perondi, E.L. Foletto, G.C. Collazzo, G.L. Dotto, Development of CO_2 activated biochar from solid wastes of a beer industry and its application for methylene blue adsorption, Waste Manage., 78 (2018) 630–638.
[12] A.F.M. Streit, L.N. Côrtes, S.P. Druzian, M. Godinho, G.C. Collazzo, D. Perondi, G.L. Dotto, Development of high-quality activated carbon from biological sludge and its application for dyes removal from aqueous solutions, Sci. Total Environ., 660 (2019) 277–287.
[13] W. Hao, F. Björnerbäck, Y. Trushkina, M.O. Bengoechea, N. Hedin, High-performance magnetic activated carbon from solid waste from lignin conversion processes. Part I: their use as adsorbents for CO_2, Energy Procedia, 114 (2017) 6272–6296.
[14] A. Raheem, V.S. Sikarwar, J. He, W. Dastyar, D.D. Dionysiou, W. Wang, M. Zhao, Opportunities and challenges in sustainable treatment and resource reuse of sewage sludge: a review, Chem. Eng. J., 337 (2018) 616–641.
[15] W. Bae, J. Kim, J. Chung, Production of granular activated carbon from food-processing wastes (walnut shells and jujube seeds) and its adsorptive properties, J. Air Waste Manage., 64 (2014) 879–886.
[16] A.M. Abioye, F.N. Ani, Recent development in the production of activated carbon electrodes from agricultural waste biomass for supercapacitors: a review, Renewable Sustainable Energy Rev., 52 (2015) 1282–1293.
[17] F. Zeng, X. Liao, D. Pan, H. Shi, Adsorption of dissolved organic matter from landfill leachate using activated carbon prepared from sewage sludge and cabbage by $ZnCl_2$, Environ. Sci. Pollut. Res. Int., 27 (2020) 4891–4904.
[18] H.B. Feng, H. Hu, H. Dong, Hierarchical structured carbon derived from bagasse wastes: a simple and efficient synthesis route and its improved electrochemical properties for high-performance supercapacitors, J. Power Sources, 302 (2016) 164–173.
[19] Y. Liu, Q. Chen, Z. Niu, X. Wang, Y. Lei, K. Yang, Preparation of peanut hull sludge-based activated carbon and application for oily wastewater treatment, Environ. Pollut. Control, 38 (2016) 43–47.
[20] S. Zhang, L. Tao, M. Jiang, G. Gou, Z. Zhou, Single-step synthesis of magnetic activated carbon from peanut shell, Mater. Lett., 157 (2015) 281–284.
[21] J. Kazmierczak-Razna, B. Gralak-Podemska, P. Nowicki, R. Pietrzak, The use of microwave radiation for obtaining activated carbons from sawdust and their potential application in removal of NO_2 and H_2S, Chem. Eng. J., 269 (2015) 352–358.
[22] G. Tan, W. Sun, Y. Xu, H. Wang, N. Xu, Sorption of mercury(II) and atrazine by biochar, modified biochars and biochar based activated carbon in aqueous solution, Bioresour. Technol., 211 (2016) 727–735.
[23] X. Zhao, W. Ouyang, F. Hao, C. Lin, F. Wang, S. Han, X. Geng, Properties comparison of biochars from corn straw with different pretreatment and sorption behaviour of atrazine, Bioresour. Technol., 147 (2013) 338–344.
[24] F.J. Gutiérrez Ortiz, P.G. Aguilera, P. Ollero, Biogas desulfurization by adsorption on thermally treated sewage-sludge, Sep. Purif. Technol., 123 (2014) 200–213.
[25] M. Seredych, T.J. Bandosz, Desulfurization of digester gas on catalytic carbonaceous adsorbents: complexity of interactions between the surface and components of the gaseous mixture, Ind. Eng. Chem. Res., 45 (2006) 3658–3665.
[26] W. Xie, L. Chang, Y.U. Jianglong, K. Xie, Research progress of removal of H_2S from coal gas by dry method, J. Chem. Ind. Eng., 9 (2012) 2012–2020.
[27] F. Zeng, X. Liao, H. Hu, L. Liao, Effect of KOH activation in the desulfurization process of activated carbon prepared by sewage sludge and corn straw, J. Air Waste Manage., 68 (2017) 255–264.
[28] F. Zeng, X. Liao, L. Liao, H. Hu, Mechanism and performance of preparation of compositional sewage sludge and corn straw-derived activated carbon with KOH, Desal. Water Treat., 108 (2018) 97–105.
[29] F. Zeng, X. Liao, Y. Li, Y. He, L. Liao, H. Hu, Preparation of sludge-straw-based activated carbon and its adsorption of H_2S, Acta Sci. Circumstantiae, 37 (2017) 4269–4276.
[30] A. Bagreev, S. Bashkova, D.C. Locke, T.J. Bandosz, Sewage sludge-derived materials as efficient adsorbents for removal of hydrogen sulfide, Environ. Sci. Technol., 35 (2001) 1537–1543.
[31] A. Ansari, A. Bagreev, T.J. Bandosz, Effect of adsorbent composition on H_2S removal on sewage sludge-based materials enriched with carbonaceous phase, Carbon, 43 (2005) 1039–1048.
[32] R. Wallace, M. Seredych, P. Zhang, T.J. Bandosz, Municipal waste conversion to hydrogen sulfide adsorbents: investigation of the synergistic effects of sewage sludge/fish waste mixture, Chem. Eng. J., 237 (2014) 88–94.
[33] X. Wang, W. Zhang, Q. Gao, Y. Wang, J. Zhang, J. Zhou, Q. Liu, G. Qian, A critical role of benzoquinone basic group in catalytic oxidation of H_2S by sewage sludge-derived catalyst, Appl. Surf. Sci., 470 (2019) 1010–1017.
[34] A. Bagreev, T.J. Bandosz, H_2S adsorption/oxidation on materials obtained using sulfuric acid activation of sewage sludge-derived fertilizer, J. Colloid Interface Sci., 252 (2002) 188–194.

[35] H. Liu, Fabrication and Modification of Activated Carbons from Biomass in Constructed Wetland and Their Adsorption Mechanisms Towards Heavy Metal Ions, Shan Dong University, 2017 (in Chinese).
[36] Y.B. Zhai, Academic Research on Adsorbent Derived from Sewage Sludge Based on Chemical Activation Method and Its Application, Hunan University, 2005 (in Chinese).
[37] X.Y. Ge, Microwave-Assisted Modification of Coal-Based Activated Carbon and Studies on PAHs Adsorption Properties, Shihezi University, 2016 (in Chinese).
[38] Y. Chen, X. Lai, Preparation and performance evaluation of iron oxide/activated carbon supported hydrogen sulfide scavenger, Ind. Catal., 22 (2014) 680–682.
[39] C.S. Zhang, W.J. Wang, H.J. Su, Z.B. Wang, E.B. Wang, Desulfurization of biogas by modified activated carbon and its regeneration, Mod. Chem. Ind., 36 (2016) 59–62.
[40] S. Pipatmanomai, S. Kaewluan, T. Vitidsant, Economic assessment of biogas-to-electricity generation system with H_2S removal by activated carbon in small pig farm, Appl. Energy, 86 (2009) 669–674.
[41] K.S.W. Sing, Reporting physisorption data for gas/solid systems with special reference to the determination of surface area and porosity, Pure Appl. Chem., 57 (1985) 603–619.
[42] S. Bashkova, F.S. Baker, X. Wu, T.R. Armstrong, V. Schwartz, Activated carbon catalyst for selective oxidation of hydrogen sulphide: on the influence of pore structure, surface characteristics, and catalytically-active nitrogen, Carbon, 45 (2007) 1354–1363.
[43] D.V. Brazhnyk, Y.P. Zaitsev, I.V. Bacherikova, V.A. Zazhigalov, J. Stoch, A. Kowal, Oxidation of H_2S on activated carbon KAU and influence of the surface state, Appl. Catal., B, 70 (2007) 557–566.
[44] S.B. Kanungo, S.K. Mishra, Thermal dehydration and decomposition of $FeCl_3 \times H_2O$, J. Therm. Anal., 46 (1996) 1487–1500.
[45] D. Wang, Q. Ma, P. Yang, Synthesis of Fe_3O_4 nanoparticles with tunable and uniform size through simple thermal decomposition, J. Nanosci. Nanotechnol., 12 (2012) 6432–6438.
[46] Z. Yang, Y. Li, X. Zhang, X. Cui, S. He, H. Liang, A. Ding, Sludge activated carbon-based $CoFe_2O_4$-SAC nanocomposites used as heterogeneous catalysts for degrading antibiotic norfloxacin through activating peroxymonosulfate, Chem. Eng. J., 384 (2020), doi: 10.1016/j.cej.2019.123319.
[47] L. Gu, H. Guo, P. Zhou, N. Zhu, D. Zhang, H. Yuan, Z. Lou, Enhanced adsorptive removal of naphthalene intermediates from aqueous solution by introducing reed straw into sewage sludge-based activated carbon, Environ. Sci. Pollut. Res., 21 (2014) 2043–2053.
[48] R. Khoshbouy, F. Takahashi, K. Yoshikawa, Preparation of high surface area sludge-based activated hydrochar via hydrothermal carbonization and application in the removal of basic dye, Environ. Res., 175 (2019) 457–467.
[49] P. Barvinschi, O. Stefanescu, T. Dippong, S. Sorescu, M. Stefanescu, $CoFe_2O_4/SiO_2$ nanocomposites by thermal decomposition of some complex combinations embedded in hybrid silica gels, J. Therm. Anal. Calorim., 112 (2013) 447–453.
[50] L. Zhang, J. Pan, L. Liu, K. Song, Q. Wang, Combined physical and chemical activation of sludge-based adsorbent enhances Cr(VI) removal from wastewater, J. Cleaner Prod., 238 (2020), doi: 10.1016/j.jclepro.2019.117904.
[51] T.L. Silva, A. Ronix, O. Pezoti, L.S. Souza, P.K.T. Leandro, K.C. Bedin, K.K. Beltrame, A.L. Cazetta, V.C. Almeida, Mesoporous activated carbon from industrial laundry sewage sludge: adsorption studies of reactive dye Remazol Brilliant Blue R, Chem. Eng. J., 303 (2016) 467–476.